International Journal of Pharmaceutics 454 (2013) 324–332

Contents lists available at SciVerse ScienceDirect

International Journal of Pharmaceutics

journal homepage: www.elsevier.com/locate/ijpharm

Consolidation trend design based on Young's modulus of clarithromycin single crystals

B. Janković[a,*], M. Škarabot[b], Z. Lavrič[a], I. Ilić[a], I. Muševič[b], S. Srčič[a], O. Planinšek[a]

[a] Department of Pharmaceutical Technology, Faculty of Pharmacy, University of Ljubljana, Ljubljana, Slovenia
[b] Department of Condensed Matter Physics, Jožef Stefan Institute, Ljubljana, Slovenia

ARTICLE INFO

Article history:
Received 14 March 2013
Accepted 4 July 2013
Available online 16 July 2013

Keywords:
Polymorphism
Clarithromycin
Atomic force microscopy
Nanoindentation
Young's modulus

ABSTRACT

The key aim of this study was to determine single mechanical properties of clarithromycin polymorphic forms in order to select some of them as more suitable for the tableting process. For this purpose, AFM single-point nanoindentation was used. The Young's moduli of clarithromycin polymorphs were substantially different, which was consistent with the structural variations in their packing motifs. The presence of the adjacent layers, which can easily slide over each other due to the low energy barrier (the lowest Young's modulus was 0.25 GPa) resulted in better bulk compressibility (the highest Heckel coefficient) of clarithromycin Form I. We also addressed the importance of tip geometry screening because the stress during the force mode often results in tip apex fracture. Even the initial manufacture of the diamond-coated tips can result in defects such as double-apex tips.

1. Introduction

Anticipating a bulk powder's compressibility based on the mechanical properties of single crystals may be beneficial for the development and formulation of solid dosage forms. Namely, intrinsic mechanical properties dictate the success of tableting, in which a predominantly elastic behavior may result in capping or lamination of tablets or increase the particle size distribution during grinding (Shariare et al., 2012). Other fundamental features of the crystal's mechanical attributes that should be taken into consideration are polymorphism, the crystal's variable habits, the existence of amorphous domains, and crystallographic defects (Brittain and Byrn, 1999; Grant, 1999). Therefore, distinct molecular packing and conformations, as well as the shape of the crystallites, determine the overall mechanical behavior of various polymorphic forms and are distinctive for pharmaceutical crystals. Clearly, plastic deformation is desirable for tableting because it contributes to permanent alteration of the particle's shape and increased contact area and binding (Sun and Grant, 2001). The fundamental principles of plastic deformation in crystals include gliding (slipping), twinning, and kinking (Sprackling, 1976). Therefore, this issue underlines the need to construct a relevant database for single mechanical properties of pharmaceutical crystals.

Clarithromycin (Clar) is a semi-synthetic macrolide antibiotic that exhibits excellent antibacterial activity against gram-positive and gram-negative bacteria, anaerobic bacteria, mycoplasma, and chlamydia. Clar exists in seven polymorphic forms designated as Form 0, Form I (Iwasaki et al., 1993), Form II (Stephenson et al., 1994), Form III (acetonitrile solvate) (Liang and Yap, 2008), Form IV (water solvate) (Avrutov et al., 2003), Form V (hydrochloride salt) (Parvez et al., 2000), and methanol solvate (Iwasaki et al., 1993). Form 0 is described as a solvate of Clar and can be prepared through recrystallization in solvents such as ethanol, isopropyl acetate, isopropanol, and tetrahydrofuran (Spanton et al., 1999). In contrast, the crystalline structures of Forms I and II result from differences in their crystal packing.

The unit cell within Forms 0, I, and II has been identified as orthorhombic (Spanton et al., 1999). Clar dosage forms currently on the market are formulated from the more stable Form II (Lui et al., 2003). On the other hand, Form I has a 3-fold faster intrinsic dissolution rate than Form II, which has implications for the prospective application of this form in new drug formulations.

Atomic force microscopy (AFM) has been widely employed to characterize the surface morphology, growth mechanisms, and surface energy of various crystalline materials (Ito et al., 2005; Picker-Freyer et al., 2007; Kiang et al., 2004; Guo and Akremitchev, 2004; Trojak et al., 2001).

With the development of nanomechanical testing, nanoindentation techniques have provided new insight into the applicable length scale of deformation in crystalline materials because a nanoindentation probe is very sensitive to the heterogeneous nature of the material being tested. Recent advances in the

* Corresponding author at: Aškerčeva 7, 1000 Ljubljana, Slovenia. Tel.: +386 1 476 9617; fax: +386 1 425 8031.
E-mail address: biljana.jankovic@ffa.uni-lj.si (B. Janković).

0378-5173/$ – see front matter © 2013 Elsevier B.V. All rights reserved.
http://dx.doi.org/10.1016/j.ijpharm.2013.07.011

manufacture of diamond-tipped AFM cantilevers with improved wear resistance and a larger tip radius have expanded the application of AFM in nanomechanical characterization of a vast range of materials. Indentation-type AFM or single-point nanoindentation is frequently used to measure the nanomechanical properties of crystals. In this mode, the tip approaches the surface and indents the sample until the set force is accomplished. After this, the tip is retracted from the surface. The data from each cycle are represented in the form of a force-versus-distance graph. Finally, by analyzing the deformation of the sample as a function of the force, the elasticity in terms of Young's modulus can be calculated (Bedoui et al., 2008; Butt et al., 2005; Cappella and Dietler, 1999; Sweers et al., 2011). The ability to visualize the morphology of the sample surface and measure Young's modulus on a small volume of material represents the crucial advantages of this technique. This is an especially important issue in the pre-formulation stage of drug development, when only a limited amount of active ingredients are available for analysis.

It is worth recalling that different polymorphic forms recrystallized from various solvents may have different physical properties such as solubility and stability. On the other hand, this paper emphasizes contrasts in their mechanical properties that make one or the other more suitable for processing (i.e., milling) and manufacturing (i.e., tableting).

In this study, the impact of polymorphism on the elasticity of Clar crystals is revealed for the very first time using AFM single-point nanoindentation. The importance of tip geometry monitoring during nanoindentation as well as tip radius determination are also addressed. Concerning the fast data throughput and reliability of the results from nanoindentation via AFM, our ultimate goal is to evaluate the method's suitability for preformulation research of pharmaceutical solids as well as quality assurance in the pharmaceutical industry.

2. Experimental

2.1. Materials

The 6-*O*-methylerythromycin A (clarithromycin) was provided by Merck, NY, USA. Acetone (Panreac Quimica, Barcelona, Spain), tetrahydrofuran (Carlo Erba, Reagents, Milan, Italy), isopropanol, and heptane (Merck, Darmstadt, Germany) were used as solvents for recrystallization.

2.2. Experimental procedures

2.2.1. Preparation of the polymorphic forms

2.2.1.1. Polymorphic Form I: recrystallization from tetrahydrofuran (THF). The process of preparing the Clar polymorphic forms represents the conversion of its solvate (Form 0) into Forms I and II by using numerous organic solvents of their mixtures and heating them at various temperatures.

A solvate of Clar was prepared by recrystallization from THF. A mixture of 7 g of the Clar sample and 20 ml of THF was warmed to reflux at 60 °C for 20 min. The clear, hot solution was than filtered (Sartorius 388 filter paper) and the filtrate was cooled slowly to ambient temperature without any mixing. This solvate was dried in a vacuum oven at 50 °C for 4 h. Large, opaque dome-shaped crystals of Form I were isolated (Lui et al., 1999).

2.2.1.2. Polymorphic Form II.

2.2.1.2.1. Recrystallization from isopropanol–heptane. A mixture of 2 g of Clar and 25 ml of isopropanol was warmed to reflux (at 68 °C) for 20 min. The hot mixture was filtered and the filtrate was heated again to 68 °C, followed by the addition of 25 ml of heptane. The solution was slowly cooled to ambient temperature. The resulting solids were collected by filtration and dried in a vacuum oven at 50 °C for 8 h. Transparent prismatic Form II crystals were isolated (Lui et al., 1999).

2.2.1.2.2. Recrystallization from THF–water mixture. A suspension of Clar (10 g) in THF (50 ml) was warmed to reflux (66 °C) for 20 min. The hot solution was filtered to remove insoluble material. The filtrate was again heated to 66 °C, followed by the addition of water (50 ml). This solution was slowly cooled to ambient temperature and the excess solvent was decanted. The resulting solid was dried in a vacuum oven at 50 °C for 8 h. Large, opaque pyramidal crystals were formed (Lui and Riley, 1998).

2.2.1.2.3. Recrystallization from acetone. A mixture of Clar (10 g) in acetone 100 ml was heated to reflux (56 °C) for 15 min. The hot solution was filtered in order to remove all remaining solids. The filtrate was then cooled slowly to ambient temperature and the excess solvent was decanted. The resulting solid was dried in a vacuum oven at 50 °C for 4 h. Large, opaque crystals the shape of rhomboid prisms were isolated (Lui and Riley, 1998).

2.2.2. Identification of crystalline forms

Differential scanning calorimetry (DSC) was used to identify polymorphic forms of Clar. DSC thermograms were recorded by a DSC 1, Mettler Toledo instrument (Columbus, OH, USA). The analysis parameters were followed: sample weight ~5 mg, placed in a covered, perforated aluminum pan, and heating rate 10 °C/min in a temperature interval from 25 to 340 °C/min under a dry nitrogen purge (50 ml/min).

2.2.3. Determination of surface and mechanical properties of Clar polymorphs

Tapping mode AFM images of crystals morphology were acquired on a Nanoscope III multimode scanning probe microscope equipped with an E-type scanner (Veeco, Santa Barbara, CA, USA). Sharp silicone probes (NTESPA5, Veeco, Santa Barbara, CA, USA) with a nominal spring constant of 42 N/m (resonance frequency 256–349 kHz) were used for imaging in tapping mode. Data were recorded at a scan rate of 1.5 Hz and stored in 512×512 pixel format. The images obtained were processed using Nanoscope software. For optimal image quality of structural details, third-order flattening was applied.

2.2.3.1. AFM nanoindentation measurements. Crystals of Clar were glued to the metallic stubs using a fast-setting epoxy adhesive (Araldit 2012, Ciba, Australia). The horizontal top crystal faces were selected for the indentation measurements.

2.2.3.1.1. Nanoindentation measurement procedure. In the nanoindentation experiment, the tip approaches and presses into the surface in order to cause a small and reversible deformation of the sample. The nanoindentation measurements involved recording the deflection-displacement curves (Fig. 1a) at different locations along the flat crystal surface. At least 150 curves were collected from different locations for each sample investigated. Curves with any inelastic contribution (hysteresis between approaching and retracting curves) were not taken into consideration.

In order to calibrate the deflection sensitivity of the cantilevers, several plots were collected on mica because neglected deformation is present in the contact zone between the AFM tip and the mica sample surface.

All measurements were performed using diamond-coated AFM tips with a nominal spring constant of 44 N/m (Nanosensors, Wetzler, Germany).

2.2.3.1.2. Data analysis. The raw deflection curves (Fig. 1a) were first converted to force separation curves (Fig. 1b) by the extrapolation of two linear segments and by using the spring constant of the cantilevers. Negative separation on these curves represents the deformation (δ) in the contact region. In the following

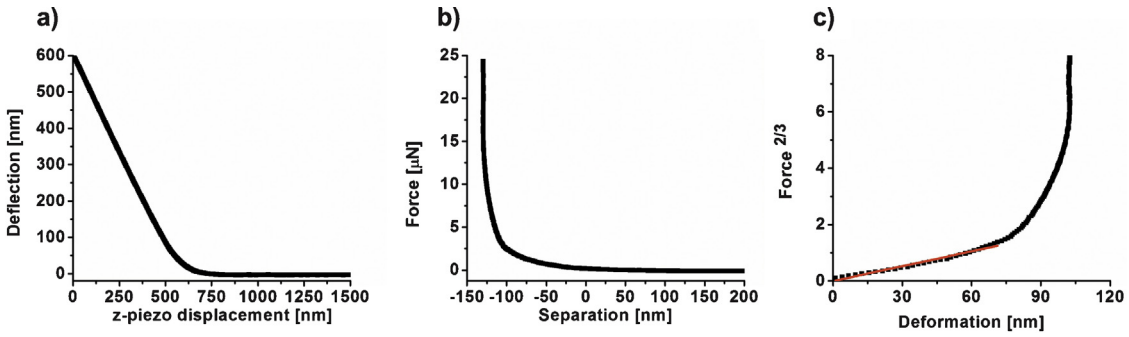

Fig. 1. AFM force curves: (a) a typical deflection versus piezo displacement curve obtained from the measurement. (b) A force-versus-separation curve obtained from the force–displacement curve. (c) Force to the power of 2/3 versus deformation.

case, the separation includes *z*-piezo displacement, cantilever deflection, and sample deformation. These curves were then converted into force-deformation curves (Fig. 1c) by indentifying the contact point. This includes determination of the zero point on the separation axis by visual inspection of the data and replotting them in the form of $F^{2/3}$ vs. deformation (δ), where linear dependence between these two values should be obtained (Fig. 1c). The contact point is deemed to be the value that gives the optimum linearity between the $F^{2/3}$ and δ.

In order to extract Young's modulus, the Hertz model was used to analyze the force curves (Hertz, 1826). Briefly, the Hertz theory neglects any adhesion between surfaces in contact, and thus only approaching curves were used for elasticity calculations.

In this model, the force between the parabolic intender and a flat surface is given by Eq. (1):

$$F = \frac{4\sqrt{R_c}}{3}\frac{E}{1-\nu^2}\delta^{3/2} \quad (1)$$

where F is the force, R_c is the radius of the tip curvature, E is Young's modulus, ν is Poisson's ratio, and δ is the deformation.

Linear segments along the $F^{2/3}$ versus δ curve were fitted to a linear equation and the coefficient r^2 value was determined for every fit, calculating Young's modulus as a function of deformation. Only fits with an r^2 over 0.95 were used in the analysis. The confidence interval for fit parameters was 95%.

The key feature for accurate calculation of Young's modulus according to the Hertz model was determination of the tip radius of curvature.

Before surface probing and after every 40 curves, probes were placed on double-sided carbon tape (diameter 12 mm, Oxon, Oxford Instruments, Oxfordshire, UK) and imaged with a scanning electron microscope (SEM) (Supra 32 VP, Zeiss, Oberkochen, Germany) with an acceleration voltage of 10 kV and a secondary electron detector. The local curvature calculation was numerically implemented using a quadratic approximation to the parabolic geometry of the tip obtained from the SEM images. The tip radius can be approximated in the apex vicinity of the parabola by $y = x^2/2R$ with a focal length of $R/2$. The curvature calculations were made with the Matlab® program.

2.2.4. Bulk mechanical properties

Because the Clar powders differed in powder size and morphology, the materials investigated were first manually ground in a mortar in order to minimize the potential effects of these variables on powder compaction properties. In order to confirm this, the median size (D 50), average size of particles (D [3,4]), and SPAN were determined, with a laser scattering–based particle sizer (Mastersizer S, Mavern Instruments, Malvern, UK).

The dispersion of powdered sample in water was pumped through the circulating flow system with a small volume dispersion unit. For better wetting of Clar powder, a few drops of 1% SDS solution were added.

Bulk mechanical properties were determined by compressing the ground pure Clar powders with a factory instrumented Killian SP300 single-punch tableting press (Killian, IMA, Cologne, Germany) with round flat-faced punches (d = 12 mm). The compression force was measured by full Wheatstone bridge strain gauges at the lower and upper punches, coupled with a linear displacement transducer mounted at the upper punch. Tablets of each sample investigated were compressed at pressures ranging from 125 to 154 MPa. Other input parameters were the following: tablet masses were approximately 745 ± 1 mg and the tableting rate was set at 25 tab/min. Tablet mass was determined using a Sartorius 1773 analytical balance (Goettingen, Germany). In addition, the true density of powdered Clar forms was measured in triplicate with a helium pycnometer (AccuPyc 1330, Micromeritics, Norcross, GA, USA).

Compressibility was evaluated using "in-die" Heckel analysis (Heckel, 1961), for which punch deformation (10.26 μm/kN) was considered and excluded by the interpretation. We are aware that the "out-die" approach is preferred for determination of bulk powder compressibility due to the exclusion of elastic determination, but the "in-die" method was utilized in this study. The main reasons for this were the strong lamination tendency of Clar powders (measuring the tablet's dimensions and porosity were infeasible) and the limited amount of powders available for this bulk compaction study. Based on our experience with pharmaceutical excipients, one measurement at different pressures is enough to obtain the relevant results for the "in-die" approach because the mean deformation properties of millions of particles are calculated (Ilić et al., 2011, 2012).

The Heckel profiles were obtained by plotting the natural logarithm of porosity ($-\ln \varepsilon$) versus compression pressure (P). The slope of the linear part of Heckel profiles (20–100 MPa) represents the rate at which porosity reduces upon increasing compression pressure and is represented by K or Heckel's coefficient. As reported in the literature, K comprises the material's compressibility (Heckel, 1961).

3. Results and discussion

3.1. Identification of the polymorphic forms

Form II was successfully prepared by recrystallization from acetone, THF/water, and isopropanol/heptane, as stated in the patent descriptions (Spanton et al., 1999; Lui et al., 2003). On the other hand, Form I was obtained only by recrystallization from a polar aprotic solvent such as THF. However, our efforts to prepare Form I from solvent mixtures such as ethanol/heptane and isopropanol/heptane were fruitless in spite of the literature data (Lui

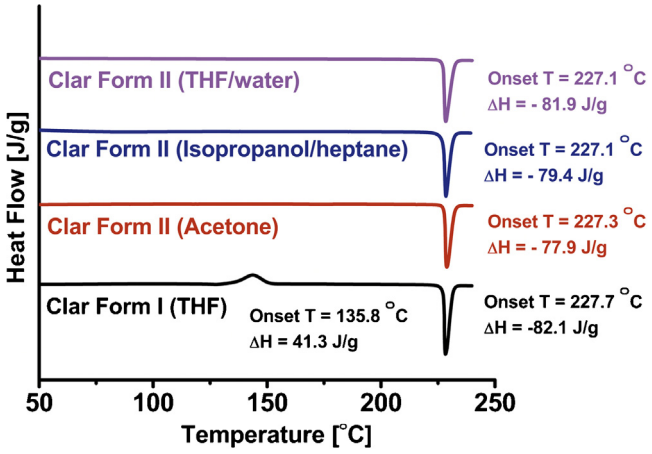

Fig. 2. Results of DSC analysis of different Clar polymorphic forms in the temperature range from 50 to 250 °C in a N_2 atmosphere. The presence of the exothermic phase-transition peak at 135.8 °C is characteristic of Form I.

et al., 2003). In this regard, involving polar protic solvents in the recrystallization procedure resulted in the isolation of the more stable Form II after the drying process.

DSC measurements confirmed the presence of Forms I and II (Fig. 2). The thermograms of Form II show only an endothermic peak at 227 °C that corresponds to the Clar melting point. On the other hand, the presence of an exothermic solid phase-transition peak at 135.8 °C was found for Form I only.

3.2. Surface and mechanical property analysis with AFM

3.2.1. Morphology characterization

It is worth recalling that slow temperature cooling was found to be the most productive approach for isolating the large Clar crystals from different solvents. All solutions were filtered in order to minimize the possibility of heterogeneous nucleation from any impurities such as dust particles. Furthermore, supersaturation was gradually reached by cooling the undersaturated solution from its elevated temperature (55–70 °C) to room temperature, and optimization of the protocol allows crystals to be grown 24 h. These large, well-defined crystals were ideal candidates for AFM experiments related to sample preparation. Fig. 3 shows the surface morphologies of Clar polymorphs. Tapping-mode AFM imaging of the dominant crystal face revealed a layered structure. Steps as well as numerous kinks along their length were observed on Clar Form II crystals prepared from acetone (Fig. 3a). The plate-like terraces between steps were formed during the single nucleation process. Moreover, layers with stacked faults were visualized on the Clar Form II surface prepared from THF/water (Fig. 3b). In addition, several molecular islands of new steps were revealed. On the other hand, a distinctly different surface morphology was noticed in the case of Clar crystals recrystallized from isopropanol/heptane (Fig. 3c). A terraced structure with parallel layers (lamellar organization) is typical for this type of crystal. According to the literature, this morphology is induced by a two-dimensional nucleation and growth mechanism (Liu et al., 2011; Piskunova and Askhabov, 2007). Comparing the morphology of these three Clar II forms shows that the number of surface irregularities and consequently the amount of roughness increases in this order: THF/water > acetone > isopropanol/heptane.

The typical surface morphology of Clar Form I is shown in Fig. 3d. The terraces are elongated in the faster growth direction and their morphology seems to suggest that growth occurs by two-dimensional nucleation.

The step heights were measured considering many sections at different height images of Clar Forms I and II. The histograms of the step heights are represented in Fig. 4. Because the data were significantly drawn from a normally distributed population according to the normality test, the median of step heights was calculated.

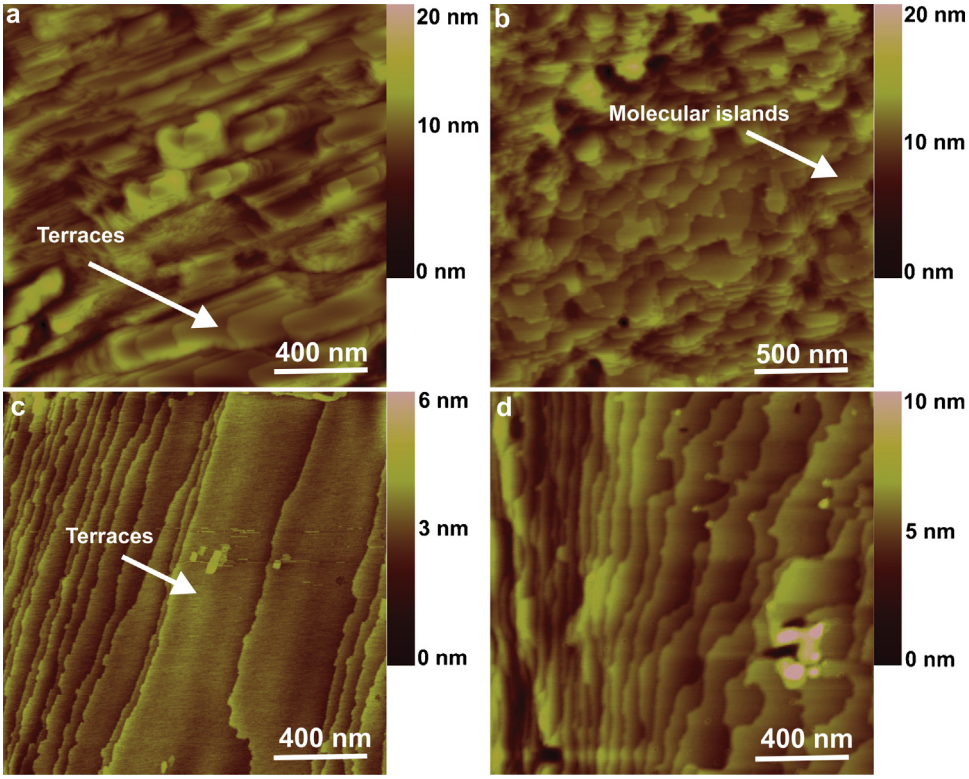

Fig. 3. Height images of Clar Form II crystals prepared from acetone (a), THF/water (b), isopropanol/heptane (c), and Form I crystals prepared from THF (d). Gradual cooling of the Clar solution in THF without mixing induced the two-dimensional nucleation and terrace-like structure of Form I (d).

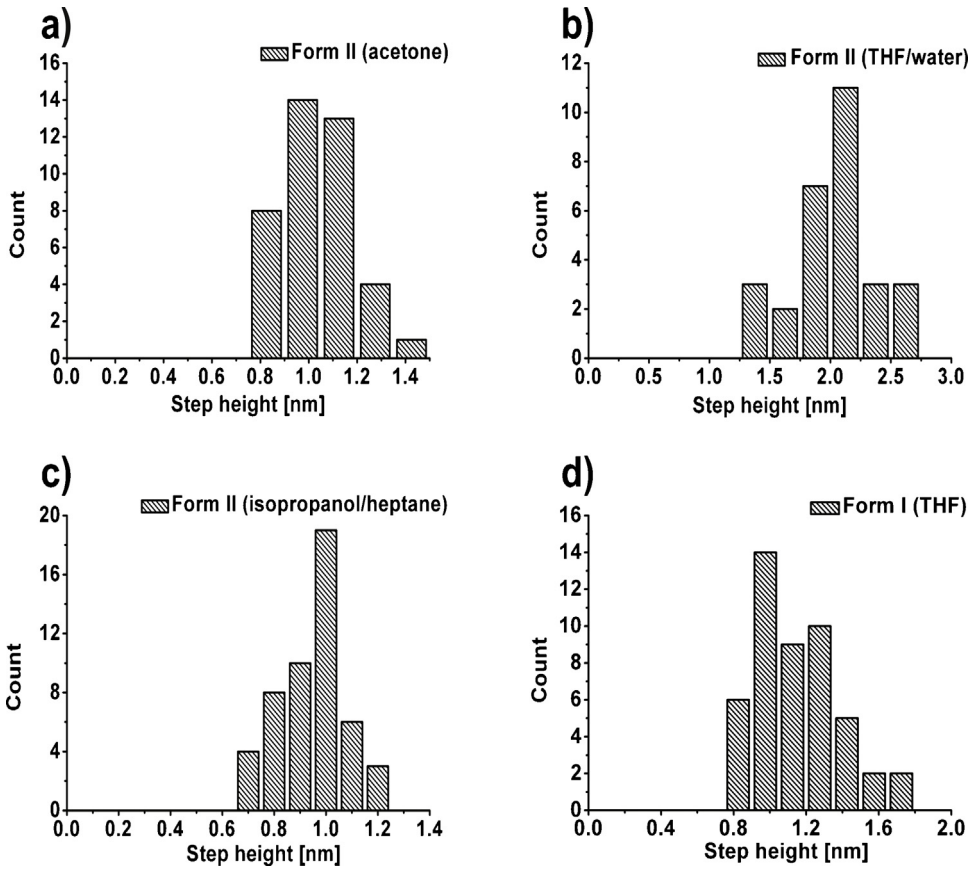

Fig. 4. Histograms of the step height measured in different sections of raw height images. (a) Form II (acetone): median step height 1.0 nm. The total number of observations is 40. (b) Form II (THF/water): median step height 2.1 nm. The total number of observations is 30. (c) Form II (isopropanol/heptane): median step height 0.9 nm. The total number of observations is 50. (d) Form I (THF): median step height 1.2 nm. The total number of observations is 50.

The dimensions of the Clar II crystal unit reported in the literature are as follows: $a = 2.0$ nm, $b = 2.4$ nm, and $c = 0.9$ nm (Iwasaki et al., 1993). Slightly different data for the Clar I crystal unit are described in the literature ($a = 1.4$ nm, $b = 3.5$ nm, and $c = 0.9$ nm) (Noguchi et al., 2012).

The step heights of 1.0 nm and 0.94 nm for the Form II isolated from acetone (Fig. 4a) and that from isopropanol/heptane (Fig. 4b), respectively, correspond well to the distance between adjacent planes (dimension c) in the crystal structure as reported in the literature (Iwasaki et al., 1993).

On the other hand, the step heights of 2.1 nm and 1.2 nm for Form II recrystallized from THF/water (Fig. 4b) and Form I (Fig. 4d) agree well with the a dimension of the crystal unit cells (2.0 nm and 1.4 nm) (Iwasaki et al., 1993; Noguchi et al., 2012).

Aside from the terrace-like structure of the crystal surfaces, roundish growth islands were also identified at the crystal surface of Form I (Fig. 5) when the solution was mixed. Steps developed by twisting around its axis during growth resulted in the spiral organization of layers (Kashchiev, 2000). This symmetry of the surface structure suggests the absence of a preferential growth direction. On the other hand, gradual cooling of the Clar solution in THF without mixing induced two-dimensional nucleation and a terrace-like structure (Fig. 3d).

3.2.2. Elastic modulus measurements

Our studies involved a few millimeter-sized crystals of Clar Forms I and II. Depending on the solvent used in the recrystallization process, crystals exhibit various habits. Dominant crystal faces were probed with the AFM tip because this area contributes most to the material's physical and mechanical properties. The Young's moduli collected from the two different crystals of each form are represented in Fig. 6 and summarized in Table 1. Because some of the data were significantly drawn from a normally distributed population according to the normality test, the medians of the Young's moduli were calculated. Namely, Clar Form I is significantly more elastic compared to Form II prepared from different solvents. Clar Form II prepared from THF/water was stiffer compared to other isomorphs (Table 1), which is connected with the 2-fold larger step height of its crystal layers.

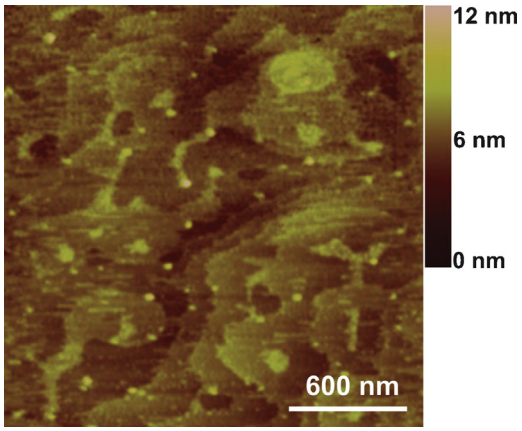

Fig. 5. Height image of the Clar Form I crystal surface. Spiral dislocations, observed at the surface of Clar Form I, are induced by mixing the solution with a magnetic stirrer during the recrystallization step.

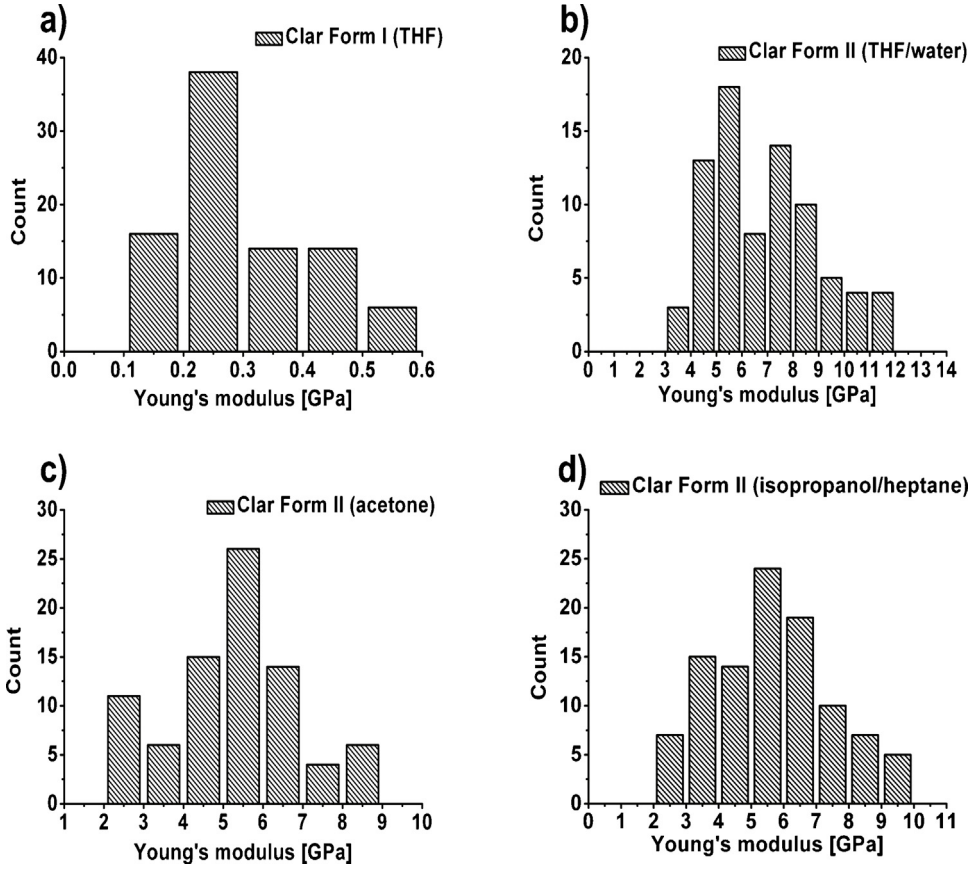

Fig. 6. Histograms of Young's moduli for: (a) Clar Form I (THF); (b) Clar Form II (THF/Water); (c) Clar Form II (acetone); and (d) Clar Form II (isopropanol/heptane).

The summary of our experimental findings was that variations in the molecular packing of the Clar polymorphic forms strongly affect the mechanical properties of its crystals; isomorphic forms have slightly different stiffness due to changes in the crystal habits; and, finally, the thermodynamically most stable polymorph is Form II, due to its higher Young's modulus (Storey and Ymén, 2011).

The reason for these results lies in the crystallographic structures of the polymorphic forms investigated. That is, the crystallographic data for Clar II demonstrate a densely zigzag arrangement of the molecules (Tian et al., 2011). In such systems, the layers within the crystals are interlocked, and consequently deformation occurs with much greater difficulty due to a larger energy barrier (Tian et al., 2011; Sun and Grant, 2001). Evidently, Clar II crystals are stiffer (i.e., they have a larger Young's modulus). On the other hand, molecules arranged in a layered packing mode are characteristic of the less stable polymorphic Form I of Clar. In addition, the Clar molecules are aligned parallel along the *a* axis in a head-to-tail manner. For this reason, the energy barrier is lower (slip between layers is favored), and, consequently, crystals are more elastic (i.e., a lower Young's modulus) (Sun and Grant, 2001).

Variations of Young's modulus were as great as several GPa and can be attributed to the different crystal unit orientations (anisotropy) and Young's modulus dependence on indentation depth; that is, depending on the number of crystal layers that the AFM tip is actually pressing. The other fact that leads to significant scattering of the results is the discrepancy in contact point determination.

3.2.3. Reliability of the AFM nanoindentation results

The AFM single-point nanoindentation approach relies on the Hertz contact model, which is, however, based on assumptions and parameters that can be determined with only limited accuracy. Poisson's ratio has minimal influence on the actual Young's modulus values. Generally, it is presumed that polymers and soft biological samples have a Poisson's ratio of 0.5, compared to 0.1–0.3 in the case of concrete materials. In our case, we used 0.3 for the calculations because the Clar crystals are classified as solid materials.

The tip radius of curvature in practice deviates from the manufacturer specification, even up to 100%. Taking this fact into consideration, it is therefore essential to measure the tip radius before and after the experiments. In our case, according to the manufacturer's specification, the tip radius was supposed to be less than 200 nm. We took SEM micrographs of the diamond-coated AFM tips and calculated the tip radii according to the procedure described in the methods section. A diversity of values for the tip radii of curvature was confirmed.

However, estimation of the tip radius in the contact zone often consists of manual thresholding. Therefore, its impact on calculation of Young's modulus according to the Hertz equation is difficult to approximate.

Aside from the tip radius, it is also important to monitor the tip geometry during nanoindentation because the tip shape can be

Table 1
Median of Young's moduli of the Clar polymorphic forms investigated.

Materials	Median of Young's modulus (GPa)	Counts
Clar Form I (THF)	0.3	91
Clar Form II (THF/water)	6.8	80
Clar Form II (acetone)	5.3	90
Clar Form II (isopropanol/heptane)	5.7	101

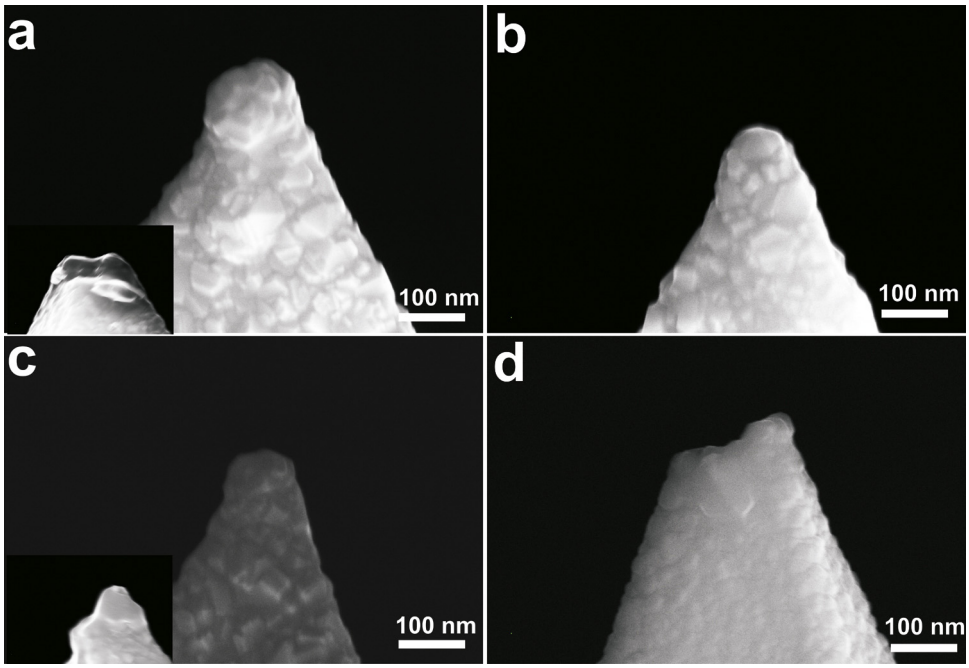

Fig. 7. SEM images of the diamond-coated AFM tips. (a) AFM tip before measurement. Magnification reveals double apex of the tip. (b) Appropriate spherical geometry of the tip. (c) Spherical AFM tip before measurements and after 40 force curves (magnification). (d) AFM Tip apex fracture.

influenced by wear (Calabri et al., 2008; Kopycinska-Muller et al., 2006). Tip geometry can be initially inappropriate due to the manufacturing process, which is evident in some cases as a double tip apex (Fig. 7a). These types of tip defects strongly affect the elasticity calculation because the Hertz theory is only valid for the sphere-on-flat model. Because the first contact between any asperity on the tip and the sample determines the zero distance (Butt et al., 2005), when there are such double-apex tips the contact point will be misinterpreted. For this reason, tip geometry screening was performed before the measurements (Fig. 7c) as well as after each of the 40 force curves (Fig. 7c magnification). On the other hand, the stress during force mode can result in fracture of the tip apex, which is illustrated in Fig. 7d. In this particular case, one can see that the tip apex was broken during nanoindentation.

An additional issue that should be considered is the deflection sensitivity variations (Guo and Akremitchev, 2004). Thus, several curves were obtained on mica in order to obtain consistent deflection sensitivity values (±5%).

Although the Hertz model provides a correct estimation of the elastic interaction forces between the tip and the sample ($r^2 > 0.95$), it generally holds only for isotropic bodies (Hertz, 1826). Clar crystals appear to be mechanically isotropic at a macroscopic scale, but they are actually anisotropic at the nanometer scale because the mechanical properties of single crystals are dependent on the orientations of the crystalline units, molecular packing, and also crystal defects. Therefore, it is essential to collect a large number of force curves (>100) for surface property mapping of anisotropic materials in order to obtain relevant results.

3.3. Bulk mechanical properties

The compaction of different Clar forms revealed pronounced tablet lamination upon ejection from the die. The origin of this phenomenon lies in extensive elastic relaxation in the decompression phase and the high elasticity of Clar crystal forms (i.e., low Young's modulus). Upon removal of the compression pressure, the stored elastic energy is released, which results in breakage of the interparticle bonds formed (i.e., the surfaces in contact at the atomic level) and eventually severe lamination. Due to this effect, the tablets' tensile strength could not be measured.

The particle size was determined using laser diffractometry in order to exclude the impact of this parameter on compression properties of Clar powders investigated. The results are given in Table 2. All Clar forms showed unimodal distribution and comparable particle size (both average D [3,4] and median D 50), as well as comparable SPAN values. Furthermore, Clar Form I showed slightly lower true density compared to Form II.

The Heckel coefficients (K), as a measure of bulk compressibility, are summarized in Table 3.

The results (Table 3) demonstrated that the most compressible powder was Clar Form I with the highest K (0.0178 MPa^{-1}) compared to the considerably poorer deformation properties of Clar II from isopropanol/heptane and acetone (0.0126–0.0129 MPa^{-1}). We also observed low porosity of Clar I at 100 MPa, confirming its higher compressibility.

Another fundamental feature was the low porosity of Clar II from THF/water at 100 MPa. This form had medium to high compressibility, but also the highest initial density observed at low pressures

Table 2
Average (D [3,4]) and median (D 50) particle sizes, SPAN, and true densities of Clar powders investigated.

Sample	D [3,4] (μm)	D 50 (μm)	SPAN	ρ_{true} (g/cm^3)
Clar Form I (THF)	257.5	188.8	0.69	1.1701
Clar Form II (THF/water)	257.8	229.8	0.57	1.1855
Clar Form II (acetone)	236.3	175.9	0.68	1.1848
Clar Form II (isopropanol/heptane)	282.2	239.1	0.58	1.1883

Table 3
Heckel analysis results of clarithromycin forms studied.

Sample	Heckel coefficient, K (MPa^{-1})	Porosity at 100 MPa (%)
Form I (THF)	0.0178	5.3
Form II (acetone)	0.0129	7.0
Form II (isopropanol/heptane)	0.0126	9.3
Form II (THF/water)	0.0165	4.9

in the Heckel profile—both effects resulting in its final low porosity during compaction (Table 3).

It should be noted that "in-die" Heckel compressibility results include both elastic and plastic deformation properties of the material studied. These two deformation mechanisms cannot be separated using the "in-die" approach; however, the validity of the "in-die" profile may be confirmed by observing the decompression curve. When correct deformation of punches and the tableting machine are taken into account, the decompression curve should be approximately horizontal, as it was in our case (data not shown).

3.4. Single versus bulk mechanical properties

One might assume that stiffer crystals (i.e., higher Young's modulus) are more desirable because they are less prone to elastic energy storage during compression and elastic relaxation in the decompression phase. On the other hand, crystals with slip planes (i.e., lower Young's modulus) are expected to have superior tableting properties because the sheets of molecules glide across one another much more easily (Sun and Hou, 2008; Karki et al., 2009).

Based on AFM measurements of Young's modulus and crystallographic data, we initially hypothesized that Form I would be more suitable for compressing. Evidently, the presence of the adjacent layers, which can easily slide over each other due to the low energy barrier (i.e., lower Young's modulus) (Table 1), yield crystals with superior bulk compressibility (i.e., the highest Heckel coefficient) of Clar Form I (Table 3).

The lack of slip planes resulted in a more rigid structure of Clar Form II isomorphs (i.e., a larger Young's modulus) (Table 1) and therefore such structures are more difficult to deform, possibly requiring higher compression pressures or a longer dwell time for sufficient plastic flow, fragmentation, and bond formation to occur.

The differences in compressibility between the Clar II forms can be attributed to numerous extrinsic factors that influence the compaction process on the bulk level, such as crystal anisotropy, presence of crystal defects, crystal habit, particle size distribution, particle shape, roughness, porosity, surface area, and many others (Nordstrom et al., 2012; Roberts and Rowe, 1987; Alderborn, 2003; Rasenack and Muller, 2002; Picker-Freyer et al., 2007; Hooton et al., 2003). The influence of extrinsic factors is especially evident in case of Clar Form II from THF/water. A greater number of surface irregularities (possibly related to a greater number of structural defects) and more roughness led to a higher Heckel coefficient compared to other isomorphs of Form II.

Nevertheless, Clar II forms display generally poorer compressibility due to their greater rigidity, determined with AFM measurements.

4. Conclusion

In summary, we introduced the AFM nanoindentation technique to compare and contrast the mechanical properties of clarithromycin polymorphic Forms I and II recrystallized from different solvents. The Young's moduli of the clarithromycin polymorphs measured were substantially different, which was consistent with the structural variations in the packing motifs. Form II is stiffer (~6.0 GPa) compared to Form I (0.3 GPa) due to the dense zigzag arrangement of layers within the crystals. These results suggested that Form I would be more suitable for tableting due to the layer organization within the crystals, which can slide more easily due to the lower energy barrier related to greater elasticity. This was confirmed at the bulk level with the superior compressibility of clarithromycin Form I (the highest Heckel coefficient). We also addressed the importance of monitoring the tip radius of curvature as well as tip geometry during AFM single-point nanoindentation studies. The tip can be fractured due to the stress during nanoindentatation, greatly contributing to uncertainties in determination of Young's modulus. Ultimately, AFM single-point nanoindentation provides the opportunity to relate the mechanical properties of actual crystals of pharmaceutical materials to their processability and to improve the performance of final dosage forms during the early pre-formulation phase.

References

Alderborn, G., 2003. A novel approach to derive a compression parameter indicating effective particle deformability. Pharm. Dev. Technol. 8, 367–377.

Avrutov, I., Lifshitz, I., Borochovitz, R., Masarwa, B., Schwartz, E., 2003. Processes for preparing clarithromycin polymorphs and novel polymorph IV. US Patent 6,599,884.

Bedoui, F., Sansoz, F., Murphy, N.S., 2008. Incidence of nanoscale heterogeneity on the nanoindentation of a semicrystalline polymer: experiments and modeling. Acta Mater. 56, 2296–2306.

Brittain, H.G., Byrn, S.R., 1999. Structural aspects of polymorphism. In: Brittain, H.G. (Ed.), Polymorphism in Pharmaceutical Solids. Marcel Dekker, New York, pp. 73–124.

Butt, H.J., Cappella, B., Kappl, M., 2005. Force measurements with the atomic force microscope: technique, interpretation and application. Surf. Sci. Rep. 59, 1–152.

Calabri, L., Pungo, N., Menozzi, C., Valeri, S., 2008. AFM nanoindentation: tip shape and tip radius of curvature effect on the hardness measurement. J. Phys. Condens. Matter 20, 474208–474215.

Cappella, B., Dietler, G., 1999. Force–distance curves by atomic force microscopy. Surf. Sci. Rep. 34, 1–104.

Grant, D.J.W., 1999. Theory and origin of polymorphism. In: Brittain, H.G. (Ed.), Polymorphism in Pharmaceutical Solids. Marcel Dekker, New York, pp. 1–33.

Guo, S., Akremitchev, B.B., 2004. Investigation of mechanical properties of insulin crystals by atomic force microscopy. Langmuir 24, 880–887.

Heckel, R.W., 1961. Density–pressure relationships in powder compression. Trans. Metall. Soc. AIME 221, 671–675.

Hertz, H., 1826. Über die Berührung fester elastischer Körper. Journal für die reine und angewandte Mathematik 92, 156–171.

Hooton, J.C., German, C.S., Allen, S., Davies, M.C., Roberts, C.J., Tendler, S.J.B., Williams, P.M., 2003. Characterization of particle interaction by atomic force microscopy: effect of contact area. Pharm. Res. 20, 508–514.

Ilić, I., Govedarica, B., Dreu, R., Srčič, S., 2011. Influence of punch deformation on models describing compressibility of powders during tableting. In: 5th International Granulation Workshop Lausanne, Switzerland.

Ilić, I., Govedarica, B., Šibanc, R., Dreu, R., Srčič, S., 2013. Deformation properties of pharmaceutical excipients determined using an in-die and out-die method. Int. J. Pharm. 446, 6–15.

Ito, A., Yamanobe-Hada, M., Shindo, H., 2005. In situ AFM observation of polymorphic transformation at crystal surface of glycine. J. Cryst. Growth 275, 1691–1695.

Iwasaki, H., Sugawara, Y., Adachi, T., Morimoto, S., Watanabe, Y., 1993. Structure of 6-*O*-methylerythromycin A (clarithromycin). Acta Crystallogr. C 49, 1227–1230.

Karki, S., Friščić, T., Fabian, L., Laity, P.R., Day, G.M., Jones, W., 2009. Improving mechanical properties of crystalline solids by cocrystal formation: new compressible forms of paracetamol. Adv. Mater. 21, 3905–3909.

Kashchiev, D., 2000. Nucleation: Basic Theory with Applications. Butterworth-Heinemann, Oxford.

Kiang, Y.H., Shi, H.G., Mathre, D.J., Zhang, W.X.D., Panmai, S., 2004. Crystal structure and surface properties of an investigational drug: a case study. Int. J. Pharm. 280, 17–26.

Kopycinska-Muller, M., Geiss, R.H., Herley, D.C., 2006. Contact mechanics and tip shape in AFM-based nanomechanical measurements. Ultramicroscopy 106, 466–474.

Liang, J.H., Yap, G.W., 2008. A new crystal structure of clarithromycin. J. Chem. Crystallogr. 38, 61–64.

Liu, G., Li, J., Chen, K., 2011. Combustion synthesis of ceramic powders with controlled grain morphologies. In: Sikalidis, C. (Ed.), Advances in Ceramics: Synthesis and Characterization, Processing and Specific Application. In Tech, Shanghai, pp. 49–70.

Lui, J.H., Henry, R.F., Spanton, S.G., Riley, G.D.A., 2003. 6-O-methylerythromycin A crystal form III. US Patent 6,627,743.

Lui, J.H., Riley, G.D.A., 1998. Preparation of crystal form II of clarithromycin. US Patent 5,844,105.

Lui, J.H., Riley, G.D.A., Spanton, S.G., 1999. Crystal form I of clarithromycin. US Patent 5,858,989.
Noguchi, S., Miura, K., Fujiki, S., Iwao, Y., Itai, S., 2012. Clarithromycin form I determined by synchrotron X-ray powder diffraction. Acta Cryst. C68, o41–o44.
Nordstrom, J., Ingvild, K., Alderborn, G., 2012. A protocol for the classification of powder compression characteristics. Eur. J. Pharm. Biopharm. 80, 209–216.
Parvez, M., Arayne, M., Sabri, S., Sultana, N., 2000. Clarithromycin hydrochloride 3.5-hydrate. Acta Cryst. C56, e398–e399.
Picker-Freyer, K.M., Liao, X., Yhang, G., Weidmann, T.S., 2007. Evaluation of the compaction of sulfathiazole polymorphs. J. Pharm. Sci. 96, 2111–2124.
Piskunova, N.N., Askhabov, A.M., 2007. AFM-observation of elementary processes of crystal growth from solution. J. Optoelectron. Adv. Mater. 9, 1290–1293.
Rasenack, N., Muller, B.W., 2002. Crystal habit and tableting behavior. Int. J. Pharm. 244, 45–57.
Roberts, R.J., Rowe, R.C., 1987. The compaction of pharmaceutical and other model materials: a pragmatic approach. Chem. Eng. Sci. 42, 903–911.
Shariare, M.H., Leusen, F.J.J., Matas, M., York, P., Anwar, J., 2012. Prediction of the mechanical behavior of crystalline solids. Pharm. Res. 29, 319–331.
Spanton, S.G., Henry, R.F., Riley, D.A., Lui, J.H., 1999. Crystal form 0 of clarithromycin. US Patent 5,945,405.
Sprackling, M.T., 1976. The Plastic Deformation of Simple Ionic Crystals. Academic Press, New York, pp. 17–19.
Stephenson, G.A., Stowell, J.G., Toma, P.H., Dorman, D.E., Greene, J.R., Byrn, S.R., 1994. Solid-state analysis of polymorphic, isomorphic and solvated forms of dirithromycin. J. Am. Chem. Soc. 116, 5766–5773.
Storey, R.A., Ymén, I., 2011. Solid state characterization of pharmaceuticals. Particulate analysis-Mechanical properties. Wiley, Chichester, pp. 375–377.
Sun, C., Grant, D.J.W., 2001. Influence of crystal structure on the tableting properties of sulfamerazine polymorphs. Pharm. Res. 18, 274–280.
Sun, C.C., Hou, H., 2008. Improving mechanical properties of caffeine and methyl gallate crystals by cocrystallization. Cryst. Growth Des. 8, 1575–1579.
Sweers, K., van der Werf, K., Bennik, M., Subramaniam, V., 2011. Nanomechanical properties of α-synuclein amyloids fibrils: a comparative study by nanoindentation harmonic force microscopy, and peakforce QNM. Nanoscale Res. Lett. 6, 1–10.
Tian, J., Dalgarno, S.J., Atwood, J.L., 2011. A new strategy of transforming pharmaceutical crystal forms. J. Am. Chem. Soc. 113, 1399–1404.
Trojak, A., Kočevar, K., Muševič, I., Srčič, S., 2001. Investigation of the felodipine glassy state by atomic force microscopy. Int. J. Pharm. 218, 145–151.